Mechanism of microstrutural modification of the interfacial transition zone by using blended materials

Kai Wu[1,2]*, Huisheng Shi[1], Geert De Schutter[2], Guang Ye[2,3], Yun Gao[2,4]

1. School of Materials Science and Engineering, Tongji University, 4800 Cao'an Road, Shanghai 201804, China

2. Magnel Laboratory for Concrete Research, Department of Structural Engineering, Ghent University, Technologiepark-Zwijnaarde 904, Ghent 9052, Belgium

3. Microlab, Faculty of Civil Engineering and Geosciences, Delft University of Technology, Stevinweg 1, CN Delft 2628, The Netherlands

4. School of Materials Science and Engineering, Southeast University, Southeast university road, Nanjing 211189, China

Abstract

Applying blended materials with finer particle size or high reactivity could be an effective and economic way for improving the microsturcture of interfacial transition zone (ITZ). In this study, the porosity characteristics of ITZ in concrete made with OPC and blended binders were determined quantitatively by using backscattered electron microscopy (BSE) image analysis and mercury intrusion porosimetry (MIP) measurements. This paper especially focused on the effects of slag and limestone filler on the thickness and pore structure of the ITZ. Results indicated that the porosity at each distance reduces with increasing limestone filler from 0 to 5%, and a significant increase is observed in the sample with 10% of limestone filler. The addition of 5% of limestone filler is able to densify the pore structure of both ITZ and bulk matrix. The reduction in pore volume in the range coarser than 100 nm contributed to the largest decrease in the total pores. Increasing the incorporation level of limestone filler to 10% resulted in an increase in the total porosity. The influences of slag on the porosity characteristics were highly dependent on the replacement level and the determined pore size regions. The addition of 35% of slag reduces the porosity at all distances and produces a denser microstructure both in the ITZ and bulk cement matrix. However, this improvement disappears when the substitution amount reaches to 70%. The incorporation of slag as a partial substitute for Portland cement tends to refine the pore structure.

Originality

Previous researches on the concrete containing blended materials mainly focus on the overall properties or on the properties of the bulk cement paste. However, very limited information has been given with respect to the improvement of the weak ITZ region by using blended materials. This work presents two possible techniques to determine the localized phenomena in concrete containing blended materials. This would also help to further understand the mechanism underlying the effects of blended materials on the structure of the ITZ, and to improve their utilization efficiency.

Keywords*: interfacial transition zone; blended materials; BSE image analysis; MIP; porosity*

[1] **Corresponding author: wukaitj@gmail.com, Tel +86-21-69582144, Fax +86-21-69582012**

1. Introduction

The microstructure of interfacial transition zone (ITZ) between aggregate and bulk cement matrix is initially determined by the packing of the anhydrous cement grains against the much larger aggregate particles. The difference in the size scale between cement grains and aggregate particles means that each aggregate particle is a mini wall which disrupts the packing of the cement grains, which leads to that the zone closest to the aggregate contains predominately small grains and has a significantly higher porosity, while larger grains are found further out (Scrivener. *et al*., 2004). The mobility of calcium ions in solution results in preferential nucleation and growth of calcium hydroxide on the aggregate surface, so that the porosity of the ITZ in many locations may be high due to the presence of these deposits. Bleeding effects may also increase porosity in other locations. In normal concrete, the ITZ is generally believed to be characterized by a higher concentration of calcium hydroxide crystals and an increased porosity relative to the matrix paste (Breton, *et al*. 1993; Bonen 1994; Scrivener. *et al*, 1996).

The formation of ITZ has been presented in Ref. (Barnes, *et al*., 1978; Barnes, Diamond *et al*. 1979; Diamond 1987) as follows: (i) at the immediate vicinity of the aggregate surface is a duplex film of $Ca(OH)_2$ topped by or occasionally intermixed with C-S-H. At early ages of hydration, this duplex film is relatively porous. With increase in age, the film modifies into a dense layer, sometimes bonding with the surrounding cement paste. The side of the film in contact with aggregate is a layer of crystalline $Ca(OH)_2$ of 0.5 μm thick. Following this layer is a thin deposit of C-S-H gel, in the form of short fiber, which extends into the cement paste. (ii) Next to the duplex film is the ITZ. This region is relatively larger with a thickness of around 50 μm, including the duplex film. Generally, this zone contains a large number of hollow-shell hydration grains, and enriched in larger $Ca(OH)_2$ crystals and ettringite (AFt). The occurrence of such a large number of hollow-shell hydration grains suggested that cement hydration is accelerated at the ITZ. This is presumable because of an availability of excess water at the vicinity of the aggregate particles. Moreover, since the growth of large crystals of $Ca(OH)_2$ and AFt is enhanced in a more open system, the occurrence of such large crystals at the ITZ is an indication of the existence of higher porosity.

The literature has highlighted the distinguishing microstructure of ITZ and its role of it plays on the properties of composites. For this reason, some efforts are needed to improve the quality of this weak region. Modification of the ITZ microstructure can be achieved by using micro-filler and pozzolanic reaction products (Scrivener. *et al*., 1988; Ollivier. *et al*., 1995; Leemann. *et al*., 2006). Such materials participate in the particle packing and longer-term pozzolanic reactions which continue to densify the ITZ. Moreover, the fine particles can also act as growth nuclei for multiple generations of CH crystals which therefore have smaller size (Xie. *et al.*,1992; Cohen. *et al*., 1994; Duan. *et al*., 2013).

Ground granulated blast-furnace slag (GGBS) is a glassy by-product of blast furnace iron making. It mainly contains calcium silicoaluminate with high reactivity (Siddique and Bennacer 2012). Appropriate use of GGBS can lead to better workability and pumpability, lower hydration heat, and reduced CO_2 emission (Siddique and Bennacer 2012; Van den Heede. *et al.*, 2012). However, incorporating GGBS generally increase total porosity while refine the pore size (Li. *et al.*, 2010; Li. *et al.*, 2014; Panesar. *et al.*, 2014). Limestone filler (LF) is one of the potential materials which can offset the negative effects of GGBS especially at early age (Carrasco. *et al.*, 2005; Mounanga. *et al.*, 2011). And Due to its technical, economical, and ecological benefits, the use of LF is also a common

practice in European countries. In general, LF improves the hydration rate of cement compounds and consequently increases the strength at early ages mainly from its physical nature. It causes a better packing of cement granular skeleton and a larger dispersion of cement grains. Additionally, LF can also act as the crystallization nucleus for the precipitation of $Ca(OH)_2$ (De Weerdt. *et al.*, 2011; Mounanga. *et al.*, 2011).

Previous researches on the concrete containing GGBS and LF mainly focus on the overall properties. However, very limited information has been given with respect to the improvement of the weak ITZ region. This paper focuses on the role of GGBS and LF on the microstructure of the ITZ. The microstructure features of ITZ in concrete with pure OPC and blended binders were determined by quantitative backscattered electron imaging (BEI) and mercury intrusion porosimetry (MIP) measurement.

2 Experiments

2.1 Materials and Mixtures

This paper considers ordinary Portland cement (CEM Type I 52.5 N), GGBS and LF as binder components. The chemical and physical characteristics of these materials are given in

Tab. 1. The sieve analysis of aggregates is given in Fig. 1.

Four series of specimens were prepared in which 35% and 70% of cement was replaced by GGBS, 5% and 10% of cement was replaced by LF. A control series was also prepared by using pure OPC. For each series, samples with systematically varied volume fraction (0, 20% and 55%), hence, varied proportions of ITZs were prepared.

All mixtures were prepared by mixing the binders with water at a fixed water to binder ratio of 0.45. After sufficient mixing and full compaction, the samples were cast into 150×150×150 mm^3. All the samples were demoulded after 24 h and then stored in the chamber with a constant temperature of 20±2°C and R.H. 95±5% until designated age.

Tab. 1 Chemical compositions of cementitious materials

Composition	OPC	GGBS	LF
	Weight (% by mass)		
CaO	63.12	40.10	-
SiO_2	18.73	35.40	0.80
Al_2O_3	4.94	11.25	0.17
MgO	1.02	7.82	0.50
Fe_2O_3	3.99	0.89	-
SO_3	3.07	0.61	-
$CaCO_3$	-	-	98.00
Loss on ignition (*LOI*, %)	2.12	0.31	43.90
Blaine fineness (m^2/kg)	353	410	753
Specific density (kg/m^3)	3092	2890	2676
Median particle size (μm)	15.7	12.5	9.4

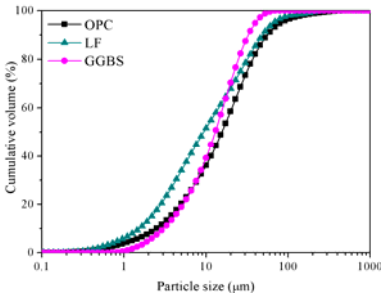

Fig. 1 Particle size distribution of the applied materials.

2.2 MIP Analysis

MIP measurements were successfully performed on mortars with systematically varied aggregate volume fraction, to detect the influence of ITZ on the porosity features (Winslow. *et al.*, 1994; Care *et al.*, 2011; Hamami. *et al.*, 2012). In this study, a systematic MIP measurement was performed on the designed blended amples of varying aggregate properties. The inner parts of the cubes were taken at designated testing age and reduced to particle samples of 1.5~3 g. Before the measurement, the collected pieces were dried by using freeze-drying procedure as indicated in elsewhere (Wu, 2014). An automatic mercury porosimeter (Thermal Scientific PASCAL 140/440 series) was used The contact angle θ of 140° and the surface tension of mercury γ of 0.480 N/m were used in the calculations.

2.3 Backscattered Electron Imaging

Scrivener and Gartner (Scrivener *et al.*, 1988) established that backscattered electron imaging (BEI) is by far the best techniques to inspect these localized phenomena. This technique was employed for its advances in providing a direct investigation and quantitative characterization, and has been proven useful for the study of ITZ microstructure (Diamond, 2001; Diamond. *et al.*, 2001; Leemann. *et al.*, 2010; Erdem. *et al.*,2012).

After 2 months of hydration, core specimens were drilled from mortars prepared with 55% of aggregate volume fraction. The obtained pieces were immersed in liquid nitrogen to stop further hydration. The dried specimens were vacuum impregnated with low viscosity epoxy resin. After epoxy drying, the samples were ground with SiC paper. Subsequently, the samples were polished with diamond paste for around 2 min each.

BSE images were acquired around random grains by using the BSE detector in the environmental scanning electron microscope with an acceleration voltage of 20 kV. Among the image analysis, it was necessary to delineate the boundary of the aggregate to specify the ITZ first. After the determination of boundary of the aggregate, a series of successive strips needs to be built starting from the surface of aggregate exactly. Within each strip, the fraction of the component versus the distance from the surface of aggregate can be given. Combining the strip delineation and phase segmentation, the phase distribution within the ITZ region can be obtained. More details on this method can be found elsewhere (Wong and Head, 2006). An example of the BEI analysis is indicated in Fig. 2. It is still worthy to mention that the threshold values for each sample are averaged from the selected images.

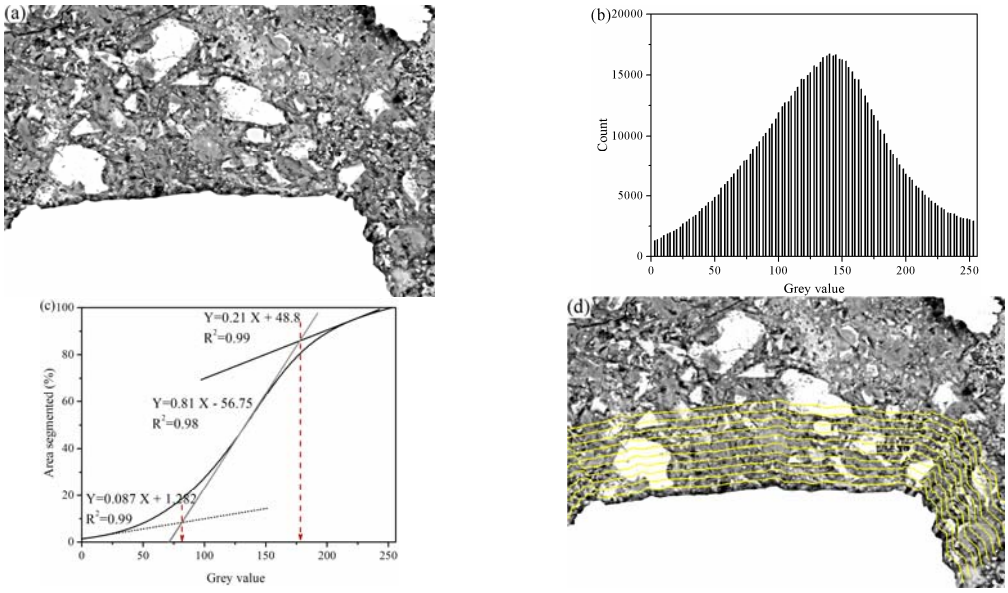

Fig. 2 Schematic view of the BSE image analysis process: (a) BSE image, (b) grey value distribution, (c) threshold value determination, (d) strips delineation.

3. Results and Discussion

3.1 BEI Analysis

The BEI examples of specimens LF-5% and LF-10% at the age of 2 months are shown in Fig. 3. Generally, LF does not posses pozzolainc properties. It only react with alumina phases of cement to form monocarboaluminate hydrate phases in relatively small quantities (De Weerdt *et al.*, 2011; Mounanga, Khokhar *et al.*, 2011). This is the reason why the LF was still observable in the samples at the age of 2 months. The calculated data for capillary porosity was given versus the distance from aggregate surface and given in Fig. 3(c). Calculated results are in line with expected trends for the typical ITZ characteristics. The porosity reaches the highest value at the interface and reduces to around 10% at a distance of 50 μm.

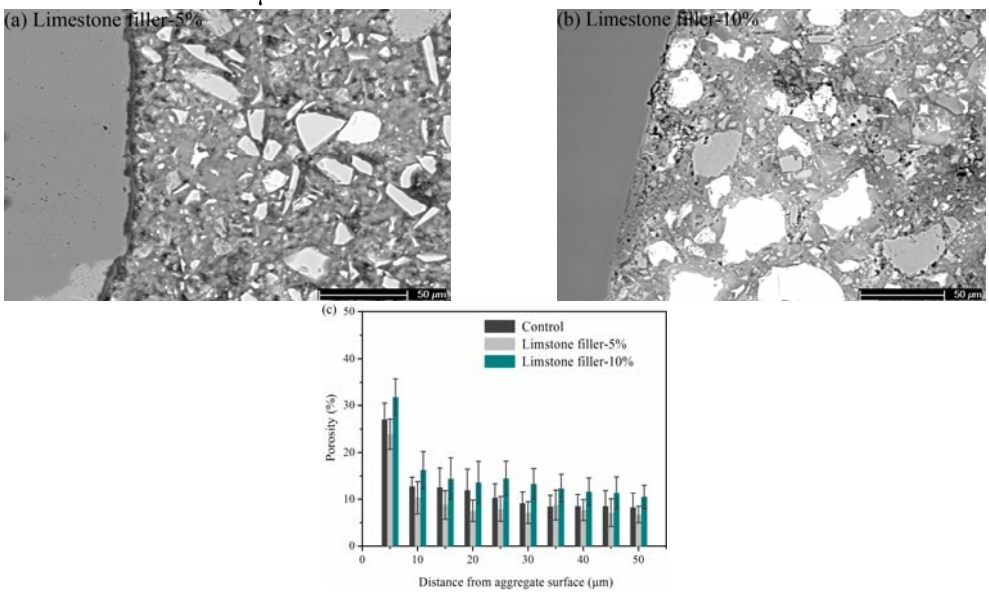

Fig. 3 Effect of limestone filler on the porosity distribution in ITZ (a) BSE image of GGBS-35%, (b) BSE image of GGBS-70%, (c) porosity distribution profile.

From Fig. 3, it can also be seen that there are remarkable differences between the control sample and the samples with LF. The porosity at each strip reduces with rising LF dosage to 5%, and a significant increase in porosity is observed in the sample blended with 10% of LF. Several effects need to be taken into account, namely (i) filler effect which causes a denser packing of cement granular skeleton and a larger dispersion of cement grains; (ii) nucleation effect which contributes to the formation of smaller CH crystals with less preferential orientations; (iii) dilution effect which reduces the quantity of cement and increases the effective w/c ratio; (iv) chemical reactions between LF and the alumina phases of cement. For LF-5%, the filler effect and nucleation effect dominate the adverse dilution effect, and produce a denser microstructure. However, increasing LF addition to 10%, the dilution effect becomes prominent and leads to a more porous structure both in the ITZ and the bulk cement matrix. Moreover, the reduction in the porosity from C-2 and L05-2 is more remarkable in the region close to aggregate (0-20 μm) than the region farther away. This may be due to the differential particle size packing.

The typical BSE images of GGBS-30% and GGBS-70% are shown in Fig. 4. From the images at high resolution, a reduced anhydrous content and size is seen in the region close to aggregate surface. The microstructure tends to compact while increasing GGBS content to 35%. On the contrary, Fig. 4(b) exhibits a more porous structure when the GGBS addition reaches to 70%. Fig. 4(c) shows the microstructural profile in relation to the substitution amount of GGBS. The porosity profiles indicate that the addition of 35% of GGBS reduces the porosity at all distances, and produces a denser microstructure both in ITZ and bulk cement matrix. However, this improvement disappears when the substitution amount reaches to 70%. The main contribution of GGBS to the development of hardened cement paste is through the pozzolanic reaction. The pozzolanic particles produce a fast saturation balance of CH, which brings to the formation of a dense cementitious matrix (Gao *et al.*, 2005). The addition of GGBS is able to decrease both the content and the arrangement of CH crystals.

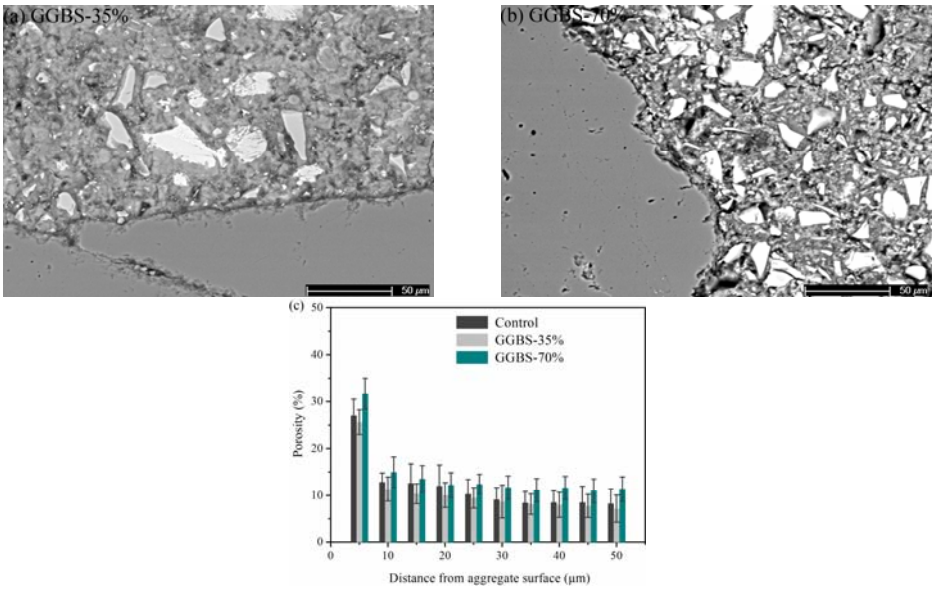

Fig. 4 Effect of GGBS on the porosity distribution in ITZ (a) BSE image of GGBS-35%, (b) BSE image of GGBS-70%, (c) porosity distribution profile.

3.2 Effect of Aggregate on the Porosity Features

To investigate the effect of aggregate volume content on the microstructure, several series of MIP tests at the curing age of 2 months have been performed. Fig. 5 presents porosity features of samples with various aggregate volume contents. These results indicate that the pore structure of specimens depends highly on the aggregate content. It can be seen in Fig. 5(a) that the pore diameters (d_1) of sample prepared with 55% of aggregate are inferior to the neat cement paste. This could be due to the fact that the bulk cement matrix is denser than the neat cement paste because of the presence of ITZ. Since the total amount of water and cement in the mortar is conserved. A lower amount of cement and greater amount of water in the ITZ would lead to a higher amount of cement and a lower amount of water in the bulk cement matrix. Another important observation is the presence of critical pores with diameter d_2 for the specimens prepared with 55% of aggregate. For the samples under this aggregate volume content, the value of d_2 is inferior to 0.5 μm. According to the previous studies (Bisschop *et al.*, 2002; Wong *et al.*, 2009), the critical pores with diameter d_2 cannot be associated with the microcrack (>1 μm) width but may be attributed to the presence of the ITZ.

The results concerning the total porosity show that the increase in the aggregate volume content decreases total porosity. This is mainly due to the reduction in the paste fraction, as the aggregates are non-porous. In order to present the results more clearly, the unit of the total porosity was transformed to mm^3/mm^3 "paste", the "paste" includes the bulk cement matrix and the ITZ. Concerning the cumulative intrusion volume in Fig. 5(b), the addition of aggregate increases total porosity, particularly at diameters larger than the thresholds of the corresponding neat cement paste. Winslow and Cohen (Winslow *et al.*, 1994) observed a sudden increase in the volume as the sand content reaches a critical value, which suggests the occurrence of percolation. The authors pointed out that as sand is added to the cement paste, ITZs are formed around each aggregate but remain relatively isolated due to the low sand content. For the mercury to reach these ITZ, it mush intrude through the denser bulk cement matrix. Some increases in the total porosity are possible to be detected due to the overlap of some ITZ with the surface of the specimen, and the critical threshold for the neat cement paste will be lost. Subsequently, as more and more aggregates are added, the isolated ITZs start to connect one to another to increase the volume of accessible ITZ. When enough aggregate is present, all the ITZ will be expected to percolate throughout the whole system.

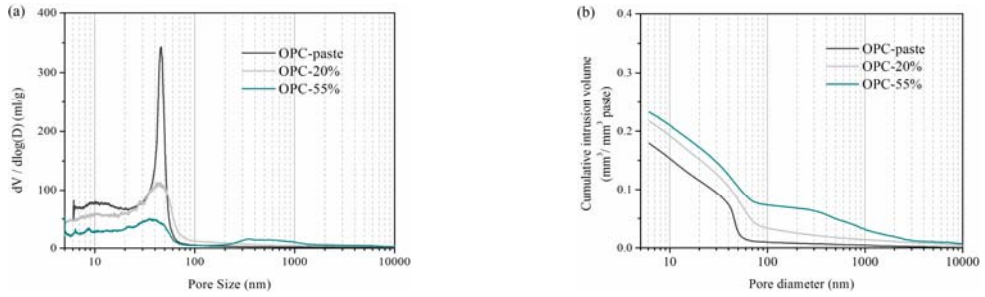

Fig. 5 PSD measured by MIP for the control series with varing aggregate content.

3.3 Effect of Blends on the Porosity Features

To clearly present the MIP results, the intruded pore volume in terms of three characteristic ranges is classified as: <10 nm (P1), 10 nm-100 nm (P2) and >100 nm (P3). To investigate the influence of blended materials, the relative differences between the intruded volume of LF-5%, LF-10% and the control samples, are calculated and given in Fig .6. A negative value represents a reduction, with a

positive value represents an increase in the pore volume. The results show that the two LF additions have different effects on the intruded pore volume. For LF-5%, 5% of LF addition leads to a decrease in the total pore volume for, P2 and P3. The reduction in P3 volume contributes to the largest decrease in the total pore volume. This indicates that the addition of 5% LF is able to modify the pore structure superior to 100 nm significantly. This confirms the improvement of the ITZ by using LF. Concerning the relative differences in the pore volume between mortars prepared with binders LF-10% and the reference, the incorporation of 10% LF increases in the total porosity and P2 pore volume, but decreases in the P3 volume. The overall pore structure is weakened, but it is still expected to have improvements in the microstructure of ITZ. This is confirmed by the reduction in P3 pore volume for LF-10%.

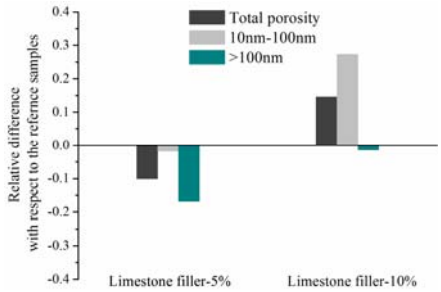

Fig. 6 Relative difference in intruded pore volume of LF blended sample with respect to the control samples.

The intruded pore volume in terms of the three pore size regions for GGBS blended samples are given in Fig. 7. Compared with the references, the effects of GGBS on the porosity are highly dependent on the replacement level and the determined classification. For GGBS-35%, the total porosity, P3 and P2 volume are less than that of GGBS-free samples, while the P1 volume is higher. Concerning the substitution of 70% GGBS for OPC, the total porosity and the P1 volume increases significantly, but the coarser pores are refined, and the P2 and P3 volume decreases. It can be concluded that the high amount of GGBS substitution can increase the total porosity but refine the pore size from the range of P3 and P2 to P1 size. The refinement for P3 pore size suggests that GGBS can densify the microstructure of ITZ. It has been proven by previous report that the size and content of CH crystals in the ITZ of GGBS blended concretes are smaller.

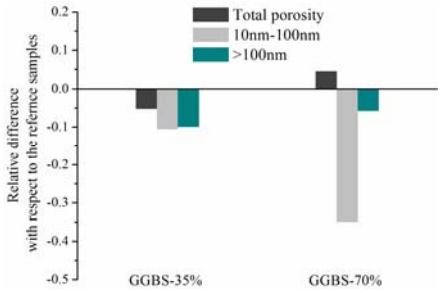

Fig. 7 Relative difference in intruded pore volume of GGBS blended sample with respect to the control samples.

To evaluate whether the reductions in transport coefficients and mechanical properties of concrete made with blended materials are mainly contributed by the modification of ITZ, or the enhancing of bulk cement matrix, the relations between the relative variations in the coefficient and the relative variations in the pore volume are presented in elsewhere (Wu, 2014). The findings indicated that the

observed improvement of impermeability of concretes with blended materials are mainly due to the imprvement in the bulk cement matrix, while the modification of mechanical properties of blended cement concrete are due to densification of ITZ microstructure.

4. Conclusions

In this study, the influences of GGBS and LF on the microstructure of the ITZ and bulk cement paste were determined. On the basis of the presented results, the main points can be summarized as:

1) For the sample prepared with 55% of aggregate, its critical pore diameters (d_1) was less than the neat cement pastes; additionally, one of the most important observations was the presence of critical pores with diameter d_2 which was superior to 0.1 μm. The total porosity increased with increasing aggregate volume fraction.

2) The incorporation of 5% of LF was able to compact the microstructure of both ITZ and bulk matrix by filling effect and nucleation sites effect. The reduction in P3 (>100 nm) volume contributed to the largest decrease in the total pore volume. However, the addition of 10% LF in substitution of OPC resulted in an increase in the total porosity and P2 (10 nm-100 nm) volume, but a decrease in the P3 volume.

3) The effects of GGBS on the porosity were highly dependent on the replacement rate and the determined pore size regions. For 35% GGBS replacement, the total porosity, P3 and P2 volume were less, while the P1 (<10 nm) volume was higher, than that of pure OPC. Concerning the substitution of 70% GGBS, the total porosity and the P1 volume increase significantly. The high amount of GGBS substitution can increase total porosity but refine the pore size from the range of P3 and P2 to P1 size.

Acknowledgement

The authors acknowledge the financial support provided by the China Scholarship Council, Special Research Fund from Ghent University, National Natural Science Foundation of China (51378390, 51402216), Program for Young Excellent Talents in Tongji University (2014KJ060) and State Key Laboratory of Pollution Control and Resource Reuse Foundation (PCRRF14009).

Reference

- Barnes, B., S. Diamond, et al., 1978. The contact zone between Portland cement paste and glass “aggregate” surfaces. *Cement and Concrete Research,* 8(2), 233-243.

- Barnes, B., S. Diamond, et al., 1979. Micromorphology of the interfacial zone around aggregates in Portland cement mortar. *Journal of the American Ceramic Society,* 62(1-2), 21-24.

- Bisschop, J., J. G. M. van Mier, 2002. Effect of aggregates on drying shrinkage microcracking in cement-based composites. *Materials and Structures* 35(252), 453-461.

- Bonen, D, 1994. Calcium hydroxide deposition in the near interfacial zone in plain concrete. *Journal of the American Ceramic Society*, 77(1), 193-196.

- Breton, D., A. Carlesgibergues, et al, 1993. Contribution to the formation mechanism of the transition zone between rock-cement Paste. *Cement and Concrete Research,* 23(2), 335-346.

- Care, S., F. Derkx, 2011. Determination of relevant parameters influencing gas permeability of mortars. *Construction and Building Materials*, 25(3), 1248-1256.

- Carrasco, M. F., G. Menendez, et al., 2005. Strength optimization of "tailor-made cement" with limestone filler and blast furnace slag. *Cement and Concrete Research,* 35(7) 1 324-1 331.

- Cohen, M. D., A. Goldman, et al., 1994. The role of silica fume in mortar- Transition zone versus bulk paste modification. *Cement and Concrete Research*, 24(1), 95-98.

- De Weerdt, K., M. Ben Haha, et al., 2011. Hydration mechanisms of ternary Portland cements containing limestone powder and fly ash. *Cement and Concrete Research,* 41(3), 279-291.
- Diamond, S., 1987. Cement paste microstructure in concrete. Microstructural development during hydration of cement. *Mater Res Soc Symp Proc*, Cambridge Univ Press.
- Diamond, S., 2001. Considerations in image analysis as applied to investigations of the ITZ in concrete. *Cement & Concrete Composites,* 23(2-3), 171-178.
- Diamond, S., J. D. Huang, 2001. The ITZ in concrete - a different view based on image analysis and SEM observations. *Cement & Concrete Composites,* 23(2-3), 179-188.
- Duan, P., Z. H. Shui, et al., 2013. Effects of metakaolin, silica fume and slag on pore structure, interfacial transition zone and compressive strength of concrete. *Construction and Building Materials,* 44, 1-6.
- Erdem, S., A. R. Dawson, et al., 2012. Influence of the micro- and nanoscale local mechanical properties of the interfacial transition zone on impact behavior of concrete made with different aggregates. *Cement and Concrete Research,* 42(2), 447-458.
- Gao, J. M., C. X. Qian, et al., 2005. ITZ microstructure of concrete containing GGBS. *Cement and Concrete Research,* 35(7), 1 299-1 304.
- Hamami, A. A., P. Turcry, et al., 2012. Influence of mix proportions on microstructure and gas permeability of cement pastes and mortars. *Cement and Concrete Research,* 42(2), 490-498.
- Leemann, A., R. Loser, et al., 2010. Influence of cement type on ITZ porosity and chloride resistance of self-compacting concrete. *Cement and Concrete Composites,* 32(2) 116-120.
- Leemann, A., B. Munch, et al., 2006. Influence of compaction on the interfacial transition zone and the permeability of concrete. *Cement and Concrete Research*, 36(8), 1 425-1 433.
- Li, K., Q. Zeng, et al., 2014. Effect of self-desiccation on the pore structure of paste and mortar incorporating 70% GGBS. *Construction and Building Materials,* 51, 329-337.
- Li, Y., J. L. Bao, et al., 2010. The relationship between autogenous shrinkage and pore structure of cement paste with mineral admixtures. *Construction and Building Materials,* 24(10), 1855-1860.
- Mounanga, P., M. I. A. Khokhar, et al., 2011. Improvement of the early-age reactivity of fly ash and blast furnace slag cementitious systems using limestone filler. *Materials and Structures,* 44(2), 437-453.
- Ollivier, J. P., J. C. Maso, et al., 1995. Interfacial transition zone in Concrete. *Advanced Cement Based Materials,* 2(1), 30-38.
- Panesar, D. K., J. Francis, 2014. Influence of limestone and slag on the pore structure of cement paste based on Mercury intrusion porosimetry and water vapour sorption measurements. *Construction and Building Materials,* 52, 52-58.
- Scrivener, K. L., A. Bentur, et al., 1988. Quantitative characterisation of the transition zone in high strength concretes. *Advanced Cement Research,* (1), 230-238.
- Scrivener, K. L., A. K. Crumbie, et al., 2004. The interfacial transition zone (ITZ) between cement paste and aggregate in concrete. *Interface Science,* 12(4), 411-421.
- Scrivener, K. L., E. M. Gartner, 1988. Microstructure gradients in cement paste and aggregate particles in bonding in cementitious composites. *Pro. Mat. Res. Sco. Symp,* (114), 77-87.
- Scrivener, K. L., K. M. Nemati, 1996. The percolation of pore space in the cement paste aggregate interfacial zone of concrete. *Cement and Concrete Research,* 26(1), 35-40.
- Siddique, R., R. Bennacer, 2012. Use of iron and steel industry by-product (GGBS) in cement paste and mortar. Resources *Conservation and Recycling*, 69, 29-34.

- Van den Heede, P., N. De Belie, 2012. Environmental impact and life cycle assessment (LCA) of traditional and 'green' concretes: Literature review and theoretical calculations. *Cement and Concrete Composites,* 34(4), 431-442.
- Winslow, D. N., M. D. Cohen, et al., 1994. Percolation and pore structure in mortars and concrete. *Cement and Concrete Research,* 24(1) 25-37.
- Wong, H. S., M. K. Head, et al., 2006. Pore segmentation of cement-based materials from backscattered electron images. *Cement and Concrete Research,* 36(6), 1 083-1 090.
- Wong, H. S., M. Zobel, et al., 2009. Influence of the interfacial transition zone and microcracking on the diffusivity, permeability and sorptivity of cement-based materials after drying. *Magazine of Concrete Research*, 61(8), 571-589.
- Wu, K., 2014. Experimental study on the influence of ITZ on the durability of concrete made with different kinds of blended materials. Department of structural engineering. Ghent, Ghent University. Ph.D.
- Xie, P., J. J. Beaudoin, 1992. Modification of transition zone microstructure - silica fume coating of aggregate surfaces. *Cement and Concrete Research*, 22(4), 597-604.